PROBING NUCLEAR COMPRESSIBILITY VIA FRAGMENTATION IN Au+Au REACTIONS AT 35A MeV

Y.K. VERMANI,[1] R. CHUGH,[1] A.D. SOOD[2]

[1]Department of Physics, Panjab University
(Chandigarh 160 014, India; e-mail: yugs80@gmail.com)

[2]SUBATECH – Ecole des Mines de Nantes
(4, rue Alfred Kastler, F-44072 Nantes, Cedex 03, France)

PACS 25.70.-z, 25.70.Pq, 24.10.Lx

The molecular dynamics study of the fragmentation in peripheral ^{197}Au+^{197}Au collisions at 35 MeV/nucleon is presented to probe the nuclear matter compressibility in the low-density regime. The yields of different fragment species, rapidity spectra, and multiplicities of charged particles with charge $3 \leq Z \leq 80$ are analyzed at different peripheral geometries employing a soft and a hard equations of state. Fragment productions are found to be quite insensitive to the choice of nucleon-nucleon cross sections allowing us to constrain the nuclear matter compressibility. The comparison of calculated charged particle multiplicities with the experimental data indicates the preference for the *soft* nature of the nuclear matter.

1. Introduction

During last two decades, the numerical simulations of medium- and high-energy heavy-ion (HI) reactions have provided a unique opportunity to explore the nuclear matter under extreme conditions of density and temperature [1–5]. The compression of the nuclear matter can be judged via the equation of state (EoS) which is also a main input for any theoretical model along with the nucleon-nucleon (n-n) cross section [4–8]. Various attempts have been made to find the observables which are sensitive to the nuclear EoS. In the past, the comparison of theoretical predictions with the experimental results has been used to extract the nuclear equation of state. One of the earlier attempts for nuclear EoS (or, incompressibility) was via giant monopole resonance (GMR) studies [9, 10]. The scattering of α-particles by a nucleus induces volume oscillations with L=0, which can be used to determine the incompressibility 'κ' of that nucleus. These results generally yield the incompressibility in the interval $\kappa \sim$ 250–270 MeV indicating the matter to be softer. A recent GMR study in the ^{208}Pb and ^{90}Zn nuclei showed that a softening of the nuclear matter is needed to explain the collective modes with different neutron-to-proton ratios [11]. Another study on the fusion reported a linear momentum transfer to be sensitive to both the EoS and n-n cross section [12]. Within the *quantum molecular dynamics* (QMD) model, the incompressibility κ = 200 MeV (i.e., soft EoS) was reported to reproduce the experimental data on the energy transfer in a compound nucleus formation [12].

The collective flow observed in HI collisions is another observable which is found to be sensitive to the stiffness of the nuclear EoS [6, 8, 13]. The collective transverse in-plane flow and the balance energy (the energy, at which the flow becomes zero) have been studied extensively over two past decades so as to constrain the EoS, but still the uncertainties are very large. For example, a stiff EoS with κ = 380 MeV reproduces the transverse flow data equally well as obtained with a soft momentum-dependent EoS with κ = 210 MeV [5, 14]. Similarly, the comparison of transport model calculations with data of EOS Collaboration for the energy dependence of the collective flow favored neither the 'soft' nor 'hard' equations of state [8]. In the recent comparison of elliptic flow data with microscopic transport model calculations in [15, 16], no consistent agreement with the data could be obtained [17] for the two different models of [15], [16]. Therefore, it is clear from the above review that an appropriate choice of the nuclear equation of state is still far from settlement. The task of deriving a quantitative information about the EoS requires a detailed comparison of theoretical calculations assuming different equations of state with experimental data.

At lower beam energies, the Pauli blocking of final states gets more pronounced. As a result, the mean-field effects and the long-range Coulomb force govern the reaction dynamics. If one goes to a still lower energy regime, the well-known phenomena like complete fusion, incomplete fusion, fission, cluster emission, *etc.* can be seen [18, 19]. At incident energies above 20A MeV, phenomena like the production of intermediate mass fragments (IMFs) and projectile-like and target-like fragments (PLFs and TLFs) dominate the exit channel. The phenomenon of multifragment-emission in the

low-energy domain is, however, least exploited to infer the nuclear EoS. Naturally, the study of the fragment-emission in the low-energy domain may be of importance to constrain the nuclear incompressibility, where the role of different n-n cross sections is expected to be minimal. To explore the possibility of achieving the information on the nuclear EoS, we plan here to simulate the peripheral reactions of ^{197}Au+^{197}Au at $E_{\rm lab}$=35A MeV and at different peripheral geometries, where accurate data has been measured on Multics-Miniball setup [20]. To this end, we performed detailed calculations within the *quantum molecular dynamics* (QMD) model [21, 22] which is described in detail in Section 2 along with a *simulated annealing clusterization algorithm* [23, 24]. Section 3 presents the results of our numerical calculations and the comparison with available experimental data which are finally summarized in Section 4.

2. Model

2.1. Quantum molecular dynamics (QMD) model

The *quantum molecular dynamics* model is an n-body transport theory that incorporates the quantum features of the Pauli blocking and the stochastic n-n scattering. Each nucleon in the colliding system is represented by a Gaussian wave packet as

$$\psi_i(\mathbf{r}, \mathbf{p}_i(t), \mathbf{r}_i(t)) = \frac{1}{(2\pi L)^{3/4}} \times$$

$$\times \exp\left[\frac{i}{\hbar}\mathbf{p}_i(t)\cdot\mathbf{r} - \frac{(\mathbf{r}-\mathbf{r}_i(t))^2}{4L}\right]. \quad (1)$$

The mean position $r_i(t)$ and the mean momentum $p_i(t)$ are two time-dependent parameters. The Gaussian width $\sqrt{L}$ is fixed with a value of 1.8 fm and is same for all nucleons. This value of $\sqrt{L}$ corresponds to the root-mean-square radius of each nucleon. The centers of these Gaussian wave packets in the $\mathcal{R}_3$ and $\mathcal{P}_3$ spaces follow the trajectories according to the classical equations of motion:

$$\dot{\mathbf{p}}_i = -\frac{\partial\langle\mathcal{H}\rangle}{\partial\mathbf{r}_i}, \quad \dot{\mathbf{r}}_i = \frac{\partial\langle\mathcal{H}\rangle}{\partial\mathbf{p}_i}. \quad (2)$$

The Skyrme parameters for 'soft' and 'hard' interactions used in the QMD model

EoS	α(MeV)	β(MeV)	γ	κ(MeV)
Soft	–356	303	7/6	200
Hard	–124	70.5	2	380

The Hamiltonian $\mathcal{H}$ appearing in Eq. (2) has contribution from the local Skyrme-type, Yukawa, and effective Coulomb interactions [21]:

$$V_{ij}^{\rm loc} = t_1\delta(\mathbf{r}_i-\mathbf{r}_j) + t_2\delta(\mathbf{r}_i-\mathbf{r}_j)\delta(\mathbf{r}_i-\mathbf{r}_k), \quad (3a)$$

$$V_{ij}^{\rm Yuk} = t_3\frac{\exp\{-|\mathbf{r}_i-\mathbf{r}_j|\}/\mu}{|\mathbf{r}_i-\mathbf{r}_j|/\mu}, \quad (3b)$$

$$V_{ij}^{\rm Coul} = \frac{Z_i\,Z_j\,e^2}{|\mathbf{r}_i-\mathbf{r}_j|}. \quad (3c)$$

Here, Z_i, Z_j are the effective charge of baryons i and j. The long-range Yukawa force is necessary to improve the surface properties of the interaction. The parameters μ, t_1, t_2, and t_3 appearing in Eqs. (3) are given in [22]. These parameters are adjusted and fitted so as to achieve the correct binding energy and the root-mean-square value of the radius of a nucleus [22]. In the QMD model, one neglects the isospin dependence of the nucleon-nucleon interaction. To all nucleons in a nucleus, we assign the effective charge $Z = \frac{Z_T+Z_P}{A_T+A_P}$ [21]. It is worth mentioning that the isospin-dependent flavor of the QMD model (i.e. IQMD) has also been used in the literature [21, 25]. This microscopic transport code explicitly takes the differences of neutron and proton potentials and cross sections into account. The Skyrme part of the interaction used in the QMD model has the generalized form:

$$V_{ij}^{\rm loc} = \frac{\alpha}{2}\left(\frac{\rho_{ij}}{\rho_\circ}\right) + \frac{\beta}{\gamma+1}\left(\frac{\rho_{ij}}{\rho_\circ}\right)^\gamma. \quad (4)$$

The interaction density in Eq. (4) is defined as

$$\rho_{ij} = \frac{1}{(4\pi L)^{3/4}}\,e^{-(\mathbf{r}_i-\mathbf{r}_j)^2/4L}. \quad (5)$$

The parameters α and β are adjusted to reproduce the infinite nuclear matter binding energy ($E/A = -16$ MeV) at the saturation nuclear matter density $\rho_\circ$. The third parameter γ can be varied independently to account for different nuclear incompressibilities κ (i.e., different equations of state). Two different parametrizations are used: a soft EoS with the incompressibility $\kappa = 200$ MeV, and a hard EoS with $\kappa = 380$ MeV. The parameters α, β, and γ employed in the QMD model serve as an input for a repulsive potential with high compressibility (i.e., the hard EoS), and a less repulsive potential (i.e., the soft EoS). The standard parameters corresponding to these two equations of state are listed in Table.

The influence of different n-n scattering cross sections will be determined by employing a set of different cross

sections varying from the energy-dependent cross section [26] to constant and isotropic cross sections with magnitudes of 40 and 55 mb. It is worth mentioning that, in recent times, even a relativistic version has also been analyzed [1]. As noted in [1], this has no effect on the present findings. A hard EoS with energy-dependent cross section is labeled as Hard$^{\rm Cg}$. The incorporation of isotropic and constant cross sections equal to 40 and 55 mb have been labeled as Hard^{40} and Hard^{55}, respectively. Similarly, for the soft equation of state, we have Soft$^{\rm Cg}$, Soft^{40}, and Soft^{55}, respectively. Since the QMD model follows the time evolution of nucleons only, one has to employ secondary clusterization algorithms to identify fragments' structure. In the present paper, the *simulated annealing clusterization algorithm* (SACA) has been used to identify the final fragment structure. This method is reported to explain the ALADiN data on the spectator fragmentation quite nicely at relativistic bombarding energies [24].

2.2. The SACA formalism

This clusterization procedure allows an early identification of fragments, before these are well separated in the coordinate space. In the SACA method, fragments are constructed based on the energy correlations. It works on the principle of minimization of the energy of the fragmenting system. The standard *minimum spanning tree* (MST) procedure [22] is employed to obtain pre-clusters. This procedure assumes that nucleon pairs separated by the distance $|\,\mathbf{r}_i-\mathbf{r}_j\,|\leq 4$ fm belong to the same fragment [6, 22]. Such preliminary cluster configuration is determined at every time step. Thus, one can address the time evolution of the mass, charge, position and momentum of each fragment or single nucleon. The pre-clusters obtained with the MST method [22, 27] are subjected to a binding energy check [23]:

$$\zeta_i = \frac{1}{N_f}\sum_{\alpha=1}^{N_f}\left[\sqrt{\left(\mathbf{p}_\alpha - \mathbf{P}_{N_f^{c.m.}}\right)^2 + m_\alpha^2} - \right.$$

$$\left. -m_\alpha + \frac{1}{2}\sum_{\beta\neq\alpha}^{N_f} V_{\alpha\beta}(\mathbf{r}_\alpha,\mathbf{r}_\beta)\right] < -E_{\rm bind}, \qquad (6)$$

with $E_{\rm bind} = 4.0$ MeV if $N_f \geq 3$, and $E_{\rm bind} = 0$ otherwise. In Eq. (6), N_f is the number of nucleons in a fragment, and $\mathbf{P}_{N_f}^{c.m.}$ is the center-of-mass momentum of the fragment. The requirement of a minimum binding energy excludes the loosely bound fragments which will decay at the later stage. To look for the most bound configuration (MBC), we start from a random configuration which is chosen by dividing the whole system into few fragments. The energy of each cluster is calculated by summing over all the nucleons present in that cluster using Eq. (6).

Let the total energy of a configuration k be $E_k(=\sum_i N_f\zeta_i)$, where N_f is the number of nucleons in a fragment, and ζ_i is the energy per nucleon of that fragment. Suppose a new configuration k' (which is obtained by (a) transferring a nucleon from a randomly chosen fragment to another fragment or by (b) setting a nucleon free, or by (c) absorbing a free nucleon into a fragment) has the total energy $E_{k'}$. If the difference between the old and new configuration energies $\Delta E(=E_{k'}-E_k)$ is negative, the new configuration is always accepted. If not, the new configuration k' may nevertheless be accepted with a probability of $\exp(-\Delta E/\upsilon)$, where υ is called the control parameter. This procedure is known as the Metropolis algorithm. The control parameter is decreased in small steps. This algorithm will yield eventually the most bound configuration (MBC). This combination of the Metropolis algorithm with a slowly decreasing control parameter υ is known as *simulated annealing*, so our approach is dubbed as the *simulated annealing clusterization algorithm* (SACA). We have used here an extended version of SACA, in which each cluster is subjected to its true binding energy based upon a modified Bethe–Weizsäcker mass formula [28]. It may be stated that the fragmentation analysis performed within the extended version yields the same results as those with a constant binding energy check of –4 MeV/nucleon. It also justifies, by using the extended approach to analyze the fragmentation at such a low incident energy, when nuclei are still in the Fermi energy domain. The constant binding energy criterion (of –4 MeV/nucleon) is chosen with regard for the average binding energy of clusters. We have also analyzed the fragmentation pattern employing $E_{\rm bind}$ based upon experimental binding energies. Nearly no effect of this modification was found. For further details, we refer the reader to [23, 24, 27, 28].

3. Results and Discussion

Figure 1 shows the time evolution of ^{197}Au $+^{197}$Au reaction at 35A MeV with the reduced impact parameters $b/b_{\rm max}$=0.55 (left panel) and 0.85 (right panel). The top panel depicts the time evolution of the average nucleon density ρ^{avg} for the soft and hard EoS. One notices several interesting results: (i) Maximal density is reached nearly at the same time at both impact param-

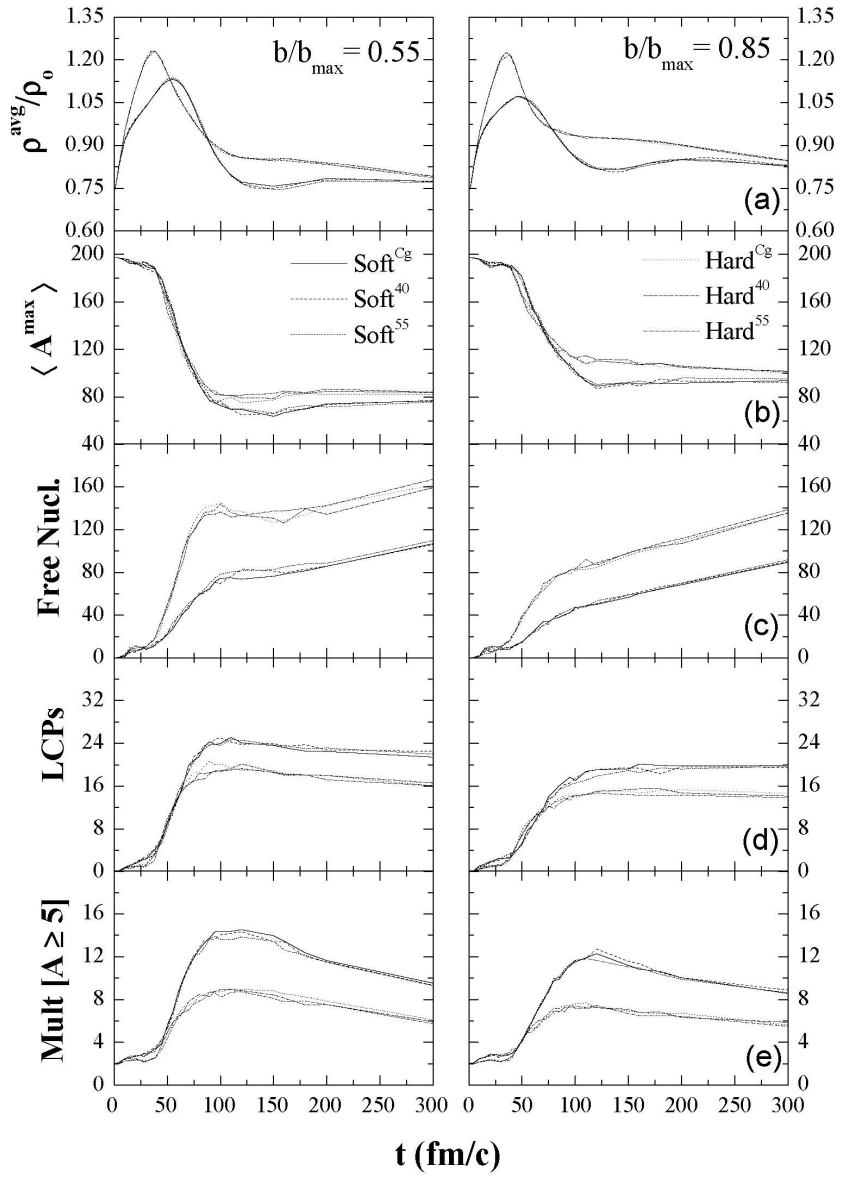

Fig. 1. QMD simulation of Au (35A MeV)+Au collisions at the reduced impact parameter $b/b_{\max}$=0.55 (left panel) and $b/b_{\max}$=0.85 (right panel) as a function of time: (*a*) mean nucleon density $\rho^{\rm avg}/\rho_o$; (b) size of the heaviest fragment $A^{\max}$; multiplicities of (*c*) free nucleons, (*d*) light charged particles LCPs, and (*e*) fragments with mass $A \geq 5$, respectively

eters, whereas the saturated value is slightly more for higher impact parameters, (ii) Choice of different *n*-*n* cross sections has insignificant influence on the results obtained. This happens due to the effective Pauli blocking at such a low incident energy that prohibits *n*-*n* collisions.

The stiffness of the nuclear EoS, however, significantly influences the mean nucleon density $\rho^{\rm avg}$ and other fragment observables shown in the subsequent windows. This difference is clearly visible in the evolution of the heaviest fragment $\langle A^{\max}\rangle$, multiplicities of free particles, light charged particles (LCPs) [$2 \leq A \leq 4$], and clusters with mass $A \geq 5$. The mean size of the heaviest fragment $\langle A^{\max}\rangle$ attains minimum around 100 fm/c, where the stable fragment configuration can be realized and compared with experimental results. With the stiff EoS, a heavier $\langle A^{\max}\rangle$ is registered. Interestingly, the multiplicity of free particles obtained also follows the same trend as $\langle A^{\max}\rangle$. This means that the dissipation of energy takes place mainly via the emission of free-nucleons,

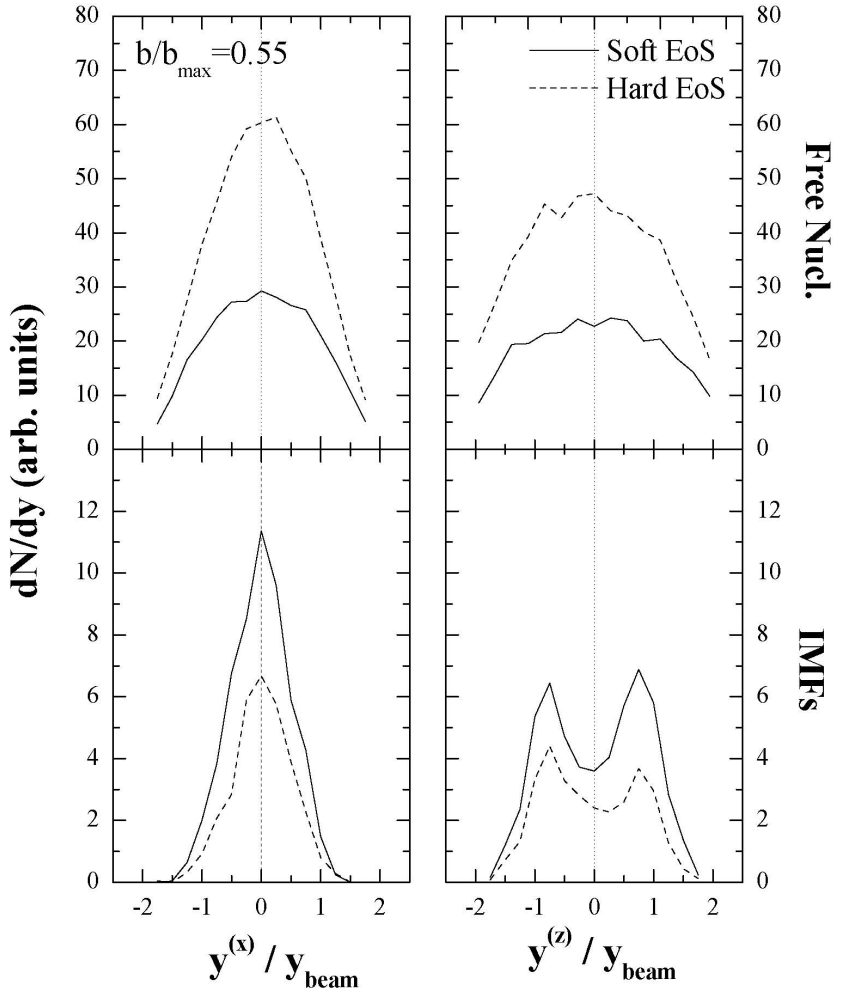

Fig. 2. Rapidity distribution $\mathrm{d}N/\mathrm{d}y$ of free nucleons and intermediate mass fragments (IMFS) as a function of the scaled transverse $y^{(x)}/y_{\mathrm{beam}}$ (left) and longitudinal $y^{(z)}/y_{\mathrm{beam}}$ (right) rapidities in Au (35A MeV)+Au reaction at the reduced impact parameter b/b_{max}=0.55. Solid and dashed curves correspond to model calculations using the 'soft' and 'hard' EoS, respectively

which cools down the nuclear system in case of the hard EoS. Consequently, the lesser yields of LCPs and fragments with mass $A \geq 5$ are obtained with the stiff EoS. On the other hand, the soft EoS favors the emission of LCPs and heavier fragments ($A \geq 5$) from the spectator zone, thereby decreasing the size of A^{max}. The insensitivity of a fragmentation pattern to the choice of different n-n cross sections may be, therefore, useful to constrain the nuclear compressibility in the low-density regime.

Next, we study the rapidity spectra of free nucleons and intermediate mass fragments in the transverse and longitudinal directions using the hard and the soft equations of state. The transfer of the excitation energy from a participant zone to the spectator matter has a direct bearing on the rapidity distribution of fragments. Figure 2 displays the spectrum of the scaled transverse $y^{(x)}$ and longitudinal $y^{(z)}$ rapidity distributions of free particles (top) and intermediate mass fragments IMFs [$5 \leq A \leq 65$] (bottom) for the collision of Au (35A MeV)+ Au at the reduced impact parameter b/b_{max}=0.55. As expected, the rapidity spectra of free nucleons and IMFs are quite sensitive to the nuclear EoS that brings out a significant change in their transverse expansion, as well as the stopping pattern. Using hard interactions, a larger fraction of free nucleons is emitted into the transverse direction. IMFs aren't, however, dispersed much into transverse directions and continue to move at target and projectile velocities. Similar trends are visible for the longitudinal rapidity (y_z) distribution as well. Using the 'stiff' EoS, the system seems to be cooled via the abundant production of free nucleons from the mid-rapidity as well as from the specta-

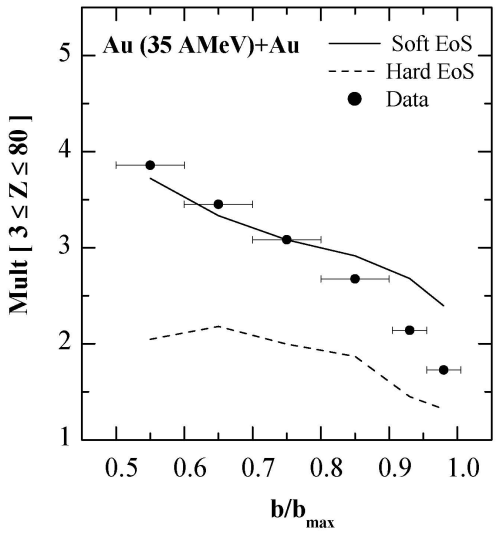

Fig. 3. Impact parameter dependence of the multiplicity of fragments with charge $3 \leq Z \leq 80$ obtained using the 'soft' EoS (solid line) and the 'hard' EoS (dashed line) in Au(35A MeV)+Au collisions. Filled circles depict the experimental data points [20]

tor zone, whereas the 'soft' EoS contributes significantly to the IMFs emission at target and projectile rapidities. This means that the system propagating under the soft interactions is less equilibrated. As a result, heavier fragments leave the participant zone quite early and suffer less collisions. These findings suggest that the fragment emission from the decay of the spectator component is quite sensitive to the mean field and the compressibility of a participant matter.

Finally, we calculate the multiplicity of charged particles with $3 \leq Z \leq 80$ using the hard and soft equations of state for Au(35A MeV)+Au collisions at six peripheral geometries (see Fig. 3). The multiplicities calculated at 100 fm/c are subjected to the forward rapidity condition ($y > 0.5y_{\rm beam}$) in the center-of-mass frame to exclude events from the mid-rapidity and the quasitarget decay. The figure presents also the integrated multiplicities of charged particles with charge $3 \leq Z \leq 80$ (i.e. $\int_3^{80} N(Z)dZ$) obtained on Multics-Miniball setup [20]. It is worth mentioning that the multiplicities were calculated with regard for the angular range covered by the combined Multics-Miniball array. We can see that the results obtained with the *soft* EoS are consistent with experimental data at all colliding geometries. These findings reflects the ability of molecular dynamics approaches (QMD, in our case) to describe the reaction dynamics in the low-energy regime.

Due to the more explosive nature of the hard EoS, the spectator matter is mainly de-excited via the emission of free nucleons, and, therefore, a decline in the multiplicity of heavier clusters occurs. An increasing trend of the fragment multiplicity with centrality can be understood in terms of a greater excitation energy deposited in the spectator matter. In semiperipheral events, a larger chunk of excitation energy gets transferred to the spectator matter, thereby, leading to a rise in the multiplicity of fragments with decrease in the impact parameter. The nuclear mean-field becomes, therefore, an important factor governing the outcome of the spectator decay, while nucleon-nucleon collisions dominate the participant matter physics. This analysis clearly illustrates the relatively *soft* nature of the nuclear matter.

4. Summary

In summary, the QMD model has been used to infer the interplay of different model inputs on the fragment-emission in peripheral ^{197}Au+^{197}Au collisions at 35A MeV. We find that the choice of different nucleon-nucleon cross sections has a marginal role to play at such low incident energy. However, the multiplicity of charged particles obtained from the spectator decay are strongly influenced by the incompressibility of the nuclear matter. The hard equation of state results in the enhanced emission of free nucleons and fewer heavier fragments. The model calculations with the soft EoS are found to give encouraging results which are in accord with experimental trends. This study favors the *soft* nature of the nuclear matter.

One of the authors (Y.K.V.) acknowledges the constructive discussions with Drs. M. D' Agostino and M. Bruno. The research grant from the Indo-French Center for the Promotion of Advanced Research (IFCPAR), New Delhi, vide grant no. IFC/4104-1 is gratefully acknowledged.

1. R.K. Puri *et al.*, Nucl. Phys. A **575**, 733 (1994); E. Lehmann, R.K. Puri, A. Faessler, G. Batko, and S.W. Huang, Phys. Rev. C **51**, 2113 (1995); E. Lehmann *et al.*, Prog. Part. Nucl. Phys. **30**, 219 (1993); S.W. Huang *et al.*, Phys. Lett. B **298**, 41 (1993).
2. A. Bohnet, N. Ohtsuka, J. Aichelin, R. Linden, and A. Faessler, Nucl. Phys. A **494**, 349 (1989); D.T. Khoa *et al.*, Nucl. Phys. A **542**, 671 (1992); G.Q. Li *et al.*, Z. Phys. A **340**, 271 (1991); D.T. Khoa *et al.*, Nucl. Phys. A **548**, 102 (1992).
3. C. Fuchs, E. Lehmann, R.K. Puri, L. Sehn, A. Faessler, and H.H. Wolter, J. Phys. G: Nucl. Part. Phys. **22**, 131 (1996); S. Kumar, R.K. Puri, and J. Aichelin, Phys.

Rev. C **58**, 1618 (1998); Y.K. Vermani, S. Goyal, and R.K. Puri, Phys. Rev. C **79**, 064613 (2009).

4. A.D. Sood and R.K. Puri, Phys. Rev. C **70**, 034611 (2004); S. Kumar, S. Kumar, and R.K. Puri, Phys. Rev. C **78**, 064602 (2008); Y.K. Vermani and R.K. Puri, J. Phys. G: Nucl. Part. Phys. **36**, 105103 (2009).
5. J. Aichelin, A. Rosenhauer, G. Peilert, H. Stöcker, and W. Greiner, Phys. Rev. Lett. **58**, 1926 (1987); C. Gale, G.F. Bertsch, and S. Das Gupta, Phys. Rev. C **35**, 1666 (1987).
6. G. Peilert *et al.*, Phys. Rev. C **39**, 1402 (1989); Mod. Phys. Lett. A **3**, 459 (1988).
7. M. Berenguer *et al.*, J. Phys. G: Nucl. Part. Phys. **18**, 655 (1992).
8. M.D. Partlan *et al.*, Phys. Rev. Lett. **75**, 2100 (1995).
9. D.H. Youngblood, H.L. Clark, and Y.W. Lui, Phys. Rev. Lett **82**, 691 (1999); J. Piekarewicz, Phys. Rev. C **69**, 041301(R) (2004), and references therein.
10. M. Itoh *et al.*, Nucl. Phys. A **687**, 52 (2001).
11. B.G. Todd-Rutel and J. Piekarewicz, Phys. Rev. Lett. **95**, 122501 (2005).
12. J. Cibor, J. Łukasik, and Z. Majka, Z. Phys. A **348**, 233 (1994); F. Haddad *et al.*, Phys. Rev. C **53**, 1437 (1996).
13. D.J. Magestro, W. Bauer, and G.D. Westfall, Phys. Rev. C **62**, 041603(R) (2000).
14. Q. Pan and P. Danielewicz, Phys. Rev. Lett. **70**, 2062 (1993).
15. A.B. Larionov, W. Cassing, C. Greiner, and U. Mosel, Phys. Rev. C **62**, 064611 (2000).
16. P. Danielewicz, R. Lacey, and W.G. Lynch, Science **298**, 1592 (2002).
17. A. Andronic *et al.*, Phys. Lett. B **612**, 173 (2005).
18. R.K. Puri, P. Chattopadhyay, and R.K. Gupta, Phys. Rev. C **43**, 315 (1991); R.K. Puri and R.K. Gupta, Phys. Rev. C **45**, 1837 (1992); J. Phys. G: Nucl. Part. Phys. **18**, 903 (1992); R.K. Gupta, S. Singh, R.K. Puri, and W. Scheid, Phys. Rev. C **47**, 561 (1993); S.S. Malik *et al.*, Pramana J. Phys. **32**, 419 (1989); R.K. Puri, S.S. Malik, and R.K. Gupta, Europhys. Lett. **9**, 767 (1989); R. Arora, R.K. Puri, and R.K. Gupta, Eur. Phys. J. A **8**, 103 (2000); R.K. Puri and N.K. Dhiman, Eur. Phys. J. A **23**, 429 (2005); R.K. Gupta, M. Balasubramaniam, R.K. Puri, and W. Scheid, J. Phys. G: Nucl. Part. Phys. **26**, L23 (2000).
19. R.K. Gupta *et al.*, J. Phys. G: Nucl. Part. Phys. **18**, 1533 (1922); I. Dutt and R.K. Puri, Phys. Rev. C **81**, 047601 (2010); Phys. Rev. C **81**, 044615 (2010); Phys. Rev. C **81**, 064609 (2010); Phys. Rev. C **81**, 064608 (2010).
20. M. D'Agostino *et al.*, Nucl. Phys. A **650**, 329 (1999).
21. Ch. Hartnack *et al.*, Eur. Phys. J. A **1**, 151 (1998); A.D. Sood and R.K. Puri, Phys. Rev. C **79**, 064618 (2009).
22. J. Aichelin, Phys. Rep. **202**, 233 (1991).
23. P.B. Gossiaux, R.K. Puri, Ch. Hartnack, and J. Aichelin, Nucl. Phys. A **619**, 379 (1997); R.K. Puri and J. Aichelin, J. Comput. Phys. **162**, 245 (2000).
24. Y.K. Vermani and R.K. Puri, Europhys. Lett. **85**, 62001 (2009).
25. S. Gautam, R. Chugh, A. D. Sood, R.K. Puri, Ch. Hartnack, and J. Aichelin, J. Phys. G: Nucl. Part. Phys. **37**, 085102 (2010); S. Kumar, S. Kumar, and R.K. Puri, Phys. Rev. C **81**, 014601; Phys. Rev. C **81**, 014611 (2010).
26. J. Cugnon, T. Mizutani, and J. Vandermeulen, Nucl. Phys. A **352**, 505 (1981).
27. J. Singh and R.K. Puri, J. Phys. G: Nucl. Part. Phys. **27**, 2091 (2001).
28. Y.K. Vermani, J.K. Dhawan, S. Goyal, R.K. Puri, and J. Aichelin, J. Phys. G: Nucl. Part. Phys. **37**, 015105 (2010).

Received 22.05.10

ВИВЧЕННЯ СТИСЛИВОСТІ ЯДЕР ЗА ФРАГМЕНТАЦІЄЮ В Au+Au РЕАКЦІЯХ ПРИ 35 МЕВ/НУКЛОН

Й.К. Вермані, К. Куг, А.Д. Суд

Р е з ю м е

Методом молекулярної динаміки досліджено фрагментацію в ^{197}Au+^{197}Au зіткнень для визначення стисливості ядерної матерії за малої щільності. Виходи різних фрагментів, спектри швидкості і множинності заряджених частинок із зарядом $3 \leq Z \leq 80$ проаналізовано для різних периферичних геометрій із використанням рівнянь стану для пластичної і жорсткої ядерної матерії. Показано, що народження фрагментів невідчутне до вибору нуклон-нуклонного перетину, що дозволяє оцінити стисливість ядерної матерії. Порівняння розрахункових множинностей заряджених частинок з експериментальними даними засвідчує пластичність ядерної матерії.